molecules

MDPI

Article

An Imidazo[1,5-a]pyridine Benzopyrylium-Based NIR Fluorescent Probe with Ultra-Large Stokes Shifts for Monitoring SO_2

Renle Cui †, Caihong Liu †, Ping Zhang †, Kun Qin * and Yanqing Ge *

Department of Chemistry and Pharmaceutical Engineering, Shandong First Medical University & Shandong Academy of Medical Sciences, No. 619, Changcheng Road, Taian 271016, China
* Correspondence: wangrui@sdfmu.edu.cn (K.Q.); yqge@sdfmu.edu.cn (Y.G.)
† These authors contributed equally to this work.

Abstract: A mitochondria-targeted NIR probe based on the FRET mechanism was developed. It shows ultra-large Stokes shifts (460 nm) and emission shifts (285 nm). Furthermore, we also realized the imaging of SO_2 in living SKOV-3 cells, zebrafish and living mice which may be useful for understanding the biological roles of SO_2 in mitochondria and in vivo.

Keywords: ultra-large Stokes shifts; imidazo[1,2-a]pyridine; bioimaging; FRET; mitochondria

check for updates

Citation: Cui, R.; Liu, C.; Zhang, P.; Qin, K.; Ge, Y. An Imidazo[1,5-a]pyridine Benzopyrylium-Based NIR Fluorescent Probe with Ultra-Large Stokes Shifts for Monitoring SO_2. *Molecules* **2023**, *28*, 515. https://doi.org/10.3390/molecules28020515

Academic Editors: Haidong Li, Yao Sun, Wei Gong and Van-Nghia Nguyen

Received: 8 December 2022
Revised: 25 December 2022
Accepted: 29 December 2022
Published: 5 January 2023

1. Introduction

Sulfur dioxide, a well-known atmospheric pollutant, has been regarded as a new possible gas transmitter following NO, CO and H_2S [1–4]. It plays important roles in many physiological processes. SO_2 can dissolve easily in water to form its derivatives bisulfite (HSO_3^-) and sulfite (SO_3^{2-}), so the physiological functions of SO_2 can be attributed to its derivatives (HSO_3^-/SO_3^{2-}). However, a high level of endogenous SO_2, generated by the oxidation of H_2S and thiol-containing amino acids in mitochondria, may bring about neurological disorders, cancers and other diseases [5–8]. Hence, it is greatly important to establish sensitive and rapid methods for SO_2 detection to further gain insight into its functions in biological systems, especially in mitochondria.

Recently, fluorescent probes have become a powerful tool in biological imaging owing to their simplicity, high selectivity and small cell damage [9–12]. Different from traditional intensity-based probes, ratiometric probes are independent of the probe concentration, environment and excitation intensity [13–15]. Besides the ICT (Intramiolecular Charge Transfer)-based ratiometric probes, fluorescence resonance energy transfer (FRET)-based ratiometric probes are the most widely designed and used (Table S1). Until now, numerous FRET-based SO_2 probes have been designed and synthesized due to their large pseudo-Stokes shifts, avoiding interference of a biological background [16–25].

As classic fluorophores, hemicyanines have drawn increasing attention because of their simple synthesis and excellent response to SO_2 [26]. Their derivatives were selected as acceptors to construct FRET probes [27,28]. However, the emission of the hemicyanines is around 600 nm, which seriously limits their application in vivo. Therefore, it is of significance to search for new fluorophores, especially with NIR emission, as acceptors.

On the other hand, to build an effective FRET platform, the development of new fluorophores as donors whose emission overlaps well with the absorption of acceptors is essential. Owing to the good optical properties [29], imidazole[1,5-a]pyridines were selected as the donor to construct the FRET platform [30]. In addition, we chose benzopyran salt as the acceptor because of its NIR emission. Meanwhile, the benzopyran moiety could not only be used as a reactive site for the Michael addition reaction with SO_2 to achieve detection purposes, but it could also target mitochondria due to positive electricity. Therefore, the

designed probe IPB-RL-1 could successfully achieve its imaging of SO_2 in mitochondria in SKOV-3 cells.

2. Results and Discussion

2.1. Synthesis of IPB-RL-1

The probe IPB-RL-1 was easily prepared using a classic organic reaction, as shown in Scheme 1. The structure was confirmed by NMR and HRMS.

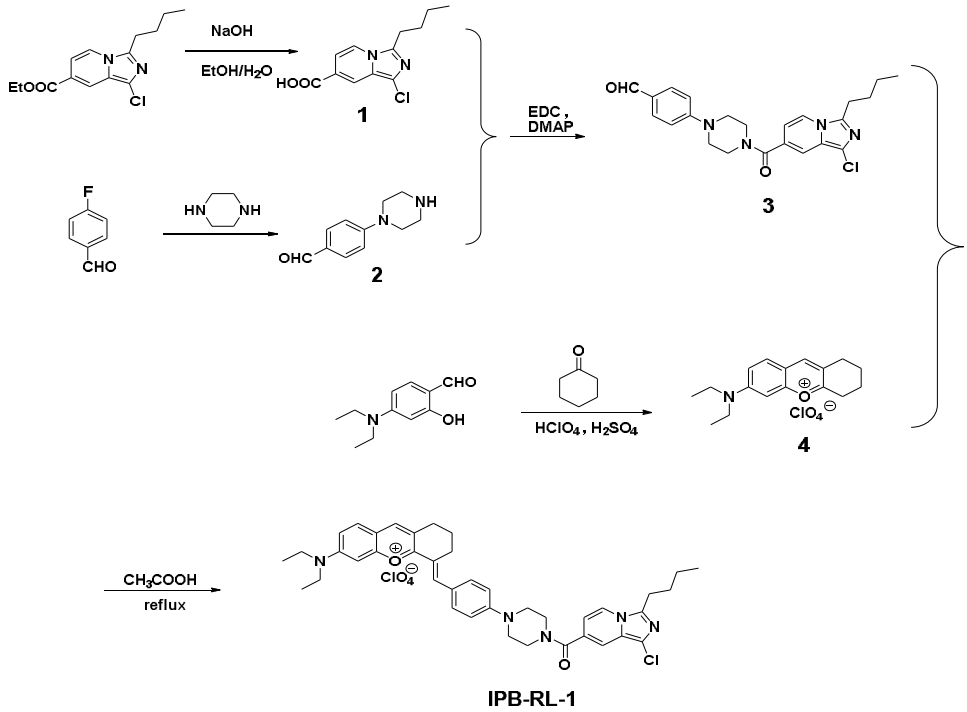

Scheme 1. Synthetic route of **IPB-RL-1**.

2.2. Optical Properties of IPB-RL-1

To examine the optical properties of **IPB-RL-1**, we first examined its selectivity. As shown in Figure 1a,b, there were no obvious changes in absorption and emission after the probe reacted with various ions (Br^-, CH_3COO^-, Cl^-, ClO_4^-, ClO^-, F^-, $H_2PO_4^-$, HCO_3^-, HPO_4^{2-}, HS^-, I^-, NO_2^-, NO_3^-, $S_2O_8^{2-}$, SO_4^{2-}, GSH, and Cys). However, when SO_3^{2-} was added, it was clearly observed by the naked eye that the probe solution changed from blue to colorless, and the fluorescence intensity was quenched at 760 nm, indicating that **IPB-RL-1** showed good selectivity for the detection of SO_3^{2-}. The anti-interference experiment (Figure S1) demonstrated that **IPB-RL-1** had good anti-interference performance and could specifically detect SO_3^{2-} even in the presence of other ions.

For a better application in living systems, UV–vis and fluorescence titration experiments were also carried out. As shown in Figure 2a, **IPB-RL-1** has a strong UV–vis absorption peak at 620 nm in the solution of DMSO/PBS (V/V = 3/7). Yet, with the continuous addition of SO_3^{2-}, the absorption peak at 620 nm decreased and the absorption peak at 310 nm increased. Meanwhile, the naked eye captured a rapid color change of the probe solution from blue to colorless. The near-infrared fluorescence emission peak at 760 nm decreased with the increase of SO_3^{2-} while the emission peak at 470 nm increased (Figure 2b), which further confirmed that the FRET was turned off. In addition, an excellent linear correlation between the ratio F_{470}/F_{760} and SO_3^{2-} concentration was observed. The detection limit was calculated to be 0.98 μM using the linear regression curve (Figure S2) and LOD formula (LOD = 3 σ/k, σ is the standard deviation of the blank measurement, and k is the slope of the fluorescence emission ratio (I_{475}/I_{760}) and SO_3^{2-} concentration). In the process of monitoring the reaction time between **IPB-RL-1** and SO_3^{2-}, the fluorescence

intensity reached equilibrium (Figure S3) in a very short time (less than 10 s). These results indicated that **IPB-RL-1** was suitable for further application in imaging in cells and in vivo.

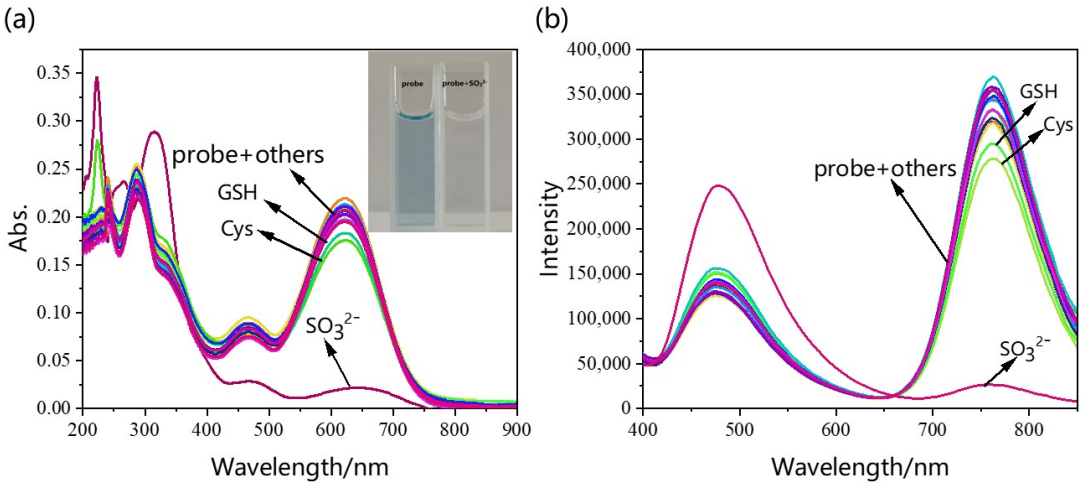

Figure 1. (**a**) UV−vis and (**b**) fluorescence spectra in response to different ions (λ_{ex} = 300 nm, slit: 5 nm/5 nm, 5 μM for fluorescence and 50 μM for UV−vis).

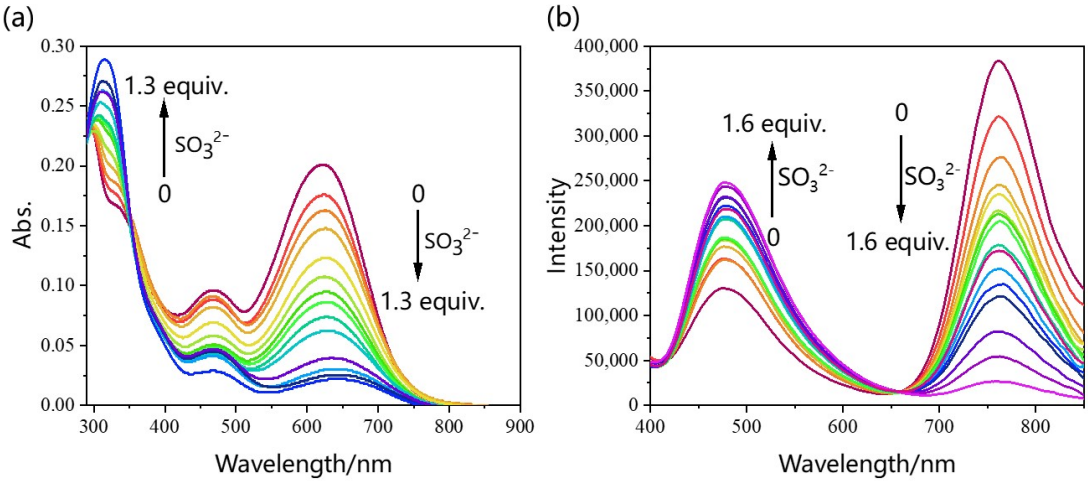

Figure 2. (**a**) UV−vis and (**b**) fluorescence spectra of **IPB-RL-1** upon the addition of SO_3^{2-} (λ_{ex} = 300 nm, slit: 5 nm/5 nm, 5 μM for fluorescence and 50 μM for UV−vis).

The results of the MTT (Methyl Thiazolyl Tetrazolium) experiment (Figure S4) showed that **IPB-RL-1** had a lower cytotoxicity to SKOV-3 cells and could be used for further cell imaging experiments. In Figure 3, fluorescence in the red and blue channels were observed after SKOV-3 cells were incubated with the probe for 1 h. However, when the cells were incubated with the probe for 1 h and then incubated with SO_3^{2-} for 20 min, the fluorescence in the blue channel was enhanced and the fluorescence in the red channel was significantly weakened, which suggested that probe **IPB-RL-1** could be used to detect SO_3^{2-} in SKOV-3 cells.

Next, since the benzopyran part of **IPB-RL-1** is positively charged, the mitochondria-targeted experiment was tested. As shown in Figure 4, the red fluorescence of MitoTracker Red and the blue fluorescence of probe **IPB-RL-1** overlap well (coefficient = 0.91).

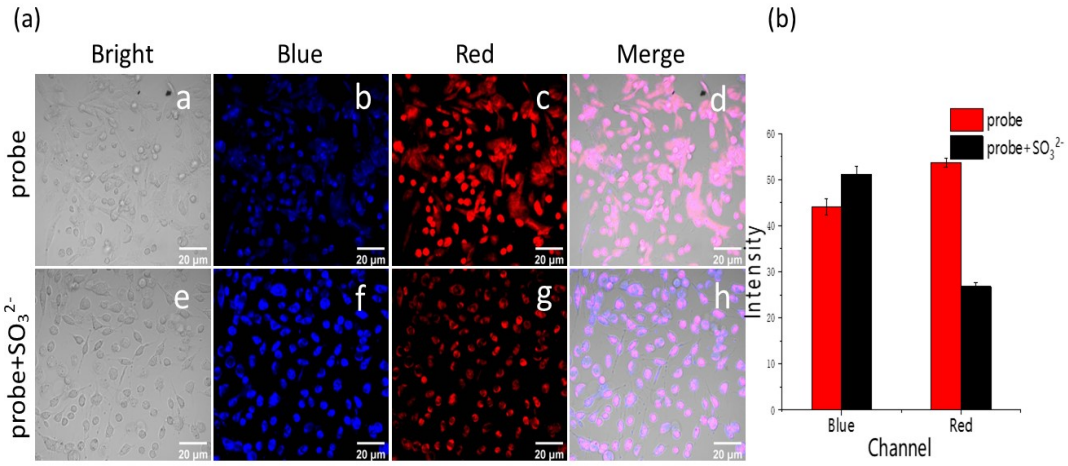

Figure 3. (**a**) Imaging of **IPB-RL-1** in SKOV-3 cells. The first row is the imaging of SKOV-3 cells incubated with **IPB-RL-1** for 30 min, and the second row is the imaging of SKOV-3 cells incubated with **IPB-RL-1** for 30 min and then treated with Na_2SO_3 for 20 min. (**b**) Comparison of the fluorescence intensity between the red channel and blue channel (λ_{ex}: 405 nm; blue: λ_{em} = 420–520 nm; red: λ_{em} = 700–800 nm).

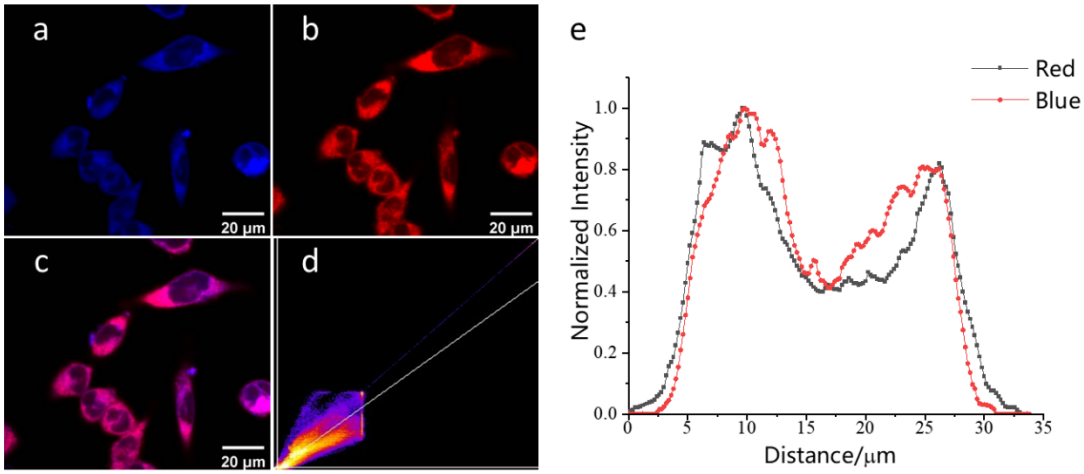

Figure 4. (**a**) Fluorescence images of **IPB-RL-1** in SKOV-3 cells (blue channel: 420–520 nm; λ_{ex}: 405 nm). (**b**) Fluorescence images of Mito-Tracker Red CMXRos (red channel: 570–620 nm; λ_{ex}: 561 nm). (**c**) Merged images of (**a**,**b**). (**d**) Images of co −location (co −location coefficient 0.91). (**e**) Fluorescence intensity of red channel and blue channel changes, respectively (λ_{ex}: 405 nm).

Owning to the excellent properties of **IPB-RL-1** in cell imaging, its capability for the visualization of SO_3^{2-} in zebrafish was examined. As depicted in Figure 5, weak blue and red fluorescent signals were observed in the control group. When the zebrafish were incubated with **IPB-RL-1** for 1 h, the fluorescent signals became obviously strong both in the blue channel and the red channel. Yet, when the zebrafish were incubated with **IPB-RL-1** for 1 h and then Na_2SO_3 for 30 min, the fluorescent signals in the red channel became obviously weak while there was no significant change in the blue channel. Therefore, we believe that **IPB-RL-1** can effectively image in vivo. Hence, imaging in mice was conducted to further explore its application advantages. As NIR fluorescence emission is required for the experiments in vivo, only fluorescence changes in the 698–766 nm range were used. As shown in Figure 6b, obvious signals were observed after the probe was injected into mice for 5 min. However, with the increase in Na_2SO_3 concentration, the fluorescence signals gradually weakened (Figure 6c,d). As the response time is less than 5 min, it is very suitable for the real-time monitoring of SO_3^{2-} in mice.

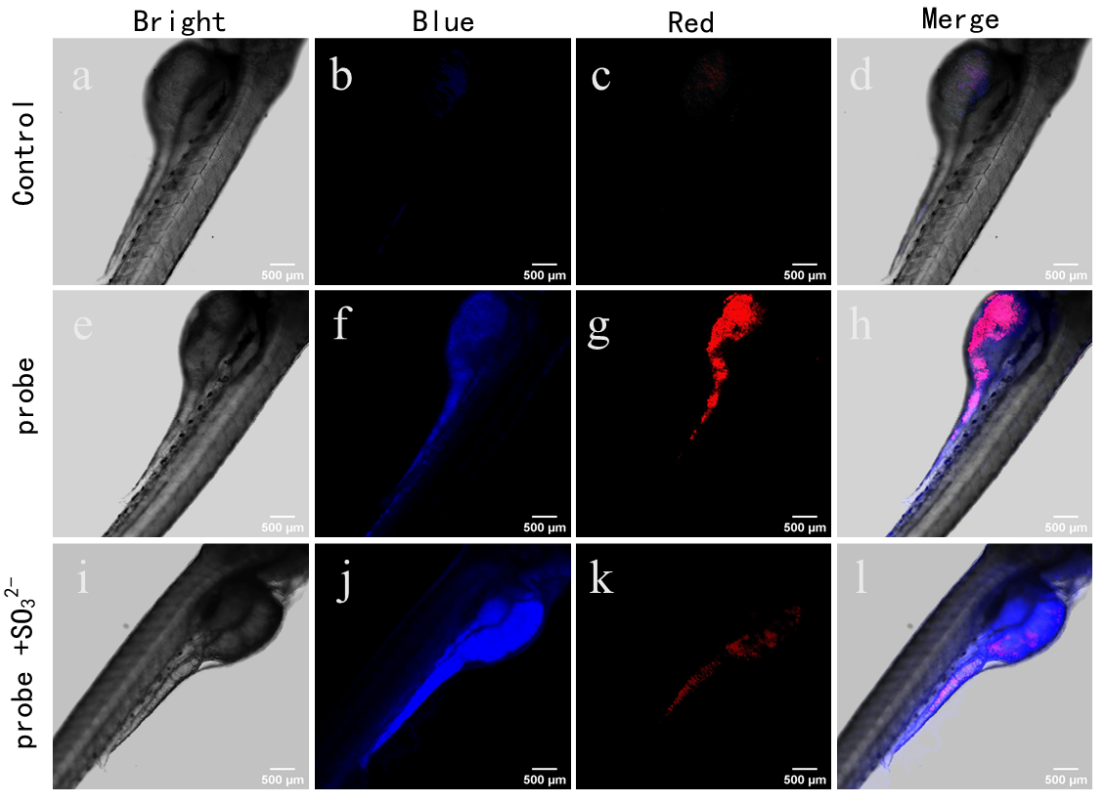

Figure 5. Fluorescence images of **IPB-RL-1** in zebrafish ((**a**−**d**): the control group; (**e**−**h**): zebrafish incubated with **IPB-RL-1** only; (**i**−**l**): zebrafish incubated with **IPB-RL-1** for 1 h and then SO_3^{2-} for 30 min; λ_{ex}: 405 nm; blue: λ_{em} = 420–520 nm; red: λ_{em} = 700–800 nm).

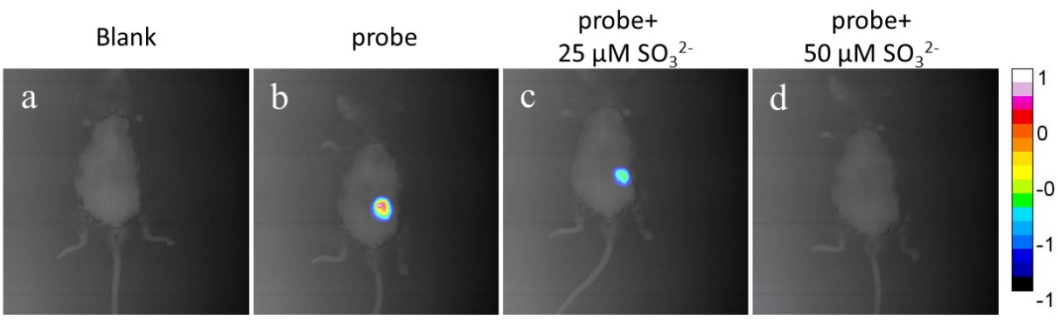

Figure 6. Fluorescence images of **IPB-RL-1** in living mice. (**a**) Images of the mice only; (**b**) images after 100 μL of 50 μM **IPB-RL-1** was injected into the mice for 5 min; (**c**) images after 100 μL of 25 μM SO_3^{2-} was injected into the mice for 5 min; (**d**) images after re-injection of 100 μL 50 μM SO_3^{2-} at the same location for 5 min (λ_{ex} = 635 nm, λ_{em} = 698–766 nm).

Based on the above results, we envisioned the mechanism of detection as follows (Scheme 2). At the excitation wavelength of 380 nm, the donor (imidazo[1,5-a]pyridine) transfers energy to the acceptor (benzopyran) and NIR fluorescence emission at 760 nm was observed. However, after the addition of SO_3^{2-}, the reaction between SO_3^{2-} and benzopyran breaks the π conjugate of benzopyran, resulting in the destruction of FRET, and thus, the energy of imidazo[1,5-a] pyridine cannot be transferred to the benzopyran. Therefore, the fluorescence emission at 760 nm disappeared and the emission at 475 nm increased. This is also confirmed by ^{1}H NMR (Figure S5).

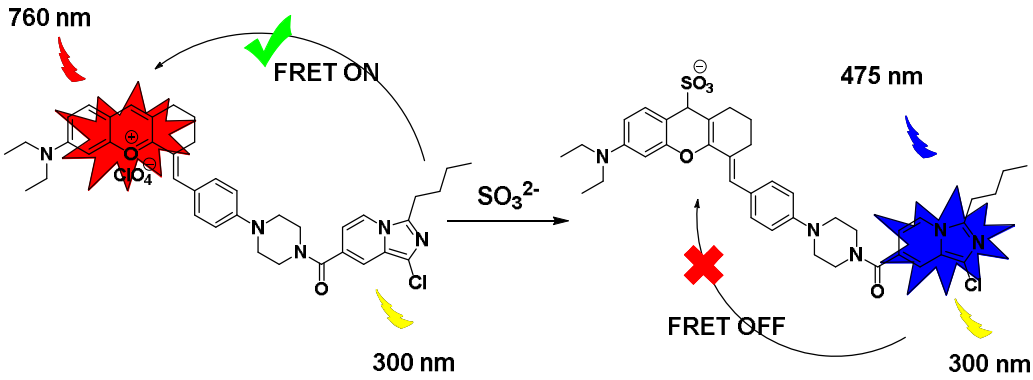

Scheme 2. Proposed mechanism.

3. Experimental

Synthesis of the Probe IPB-RL-1

As demonstrated in Scheme 1, compounds **1–4** were synthesized according to the reported procedure [9,27].

Compound **3** (0.10 g, 0.24 mmol), compound **4** (0.10 g, 0.28 mmol) and CH_3COOH (8 mL) were added to a 25 mL round-bottom flask. The mixture was heated to reflux for 3 h and then poured into water (100 mL). After being extracted with DCM (20 mL) three times, the combined organic solvent was removed under reduced pressure. The pure product was obtained by column chromatography (CH_2Cl_2:MeOH = 200:1). Black solid, ^{1}H NMR (400 MHz, DMSO-d_6) δ: 8.36 (s, 1H), 8.22 (d, J = 7.2 Hz, 1H), 8.00 (s, 1H), 7.78 (s, 1H), 7.59 (d, J = 8.8 Hz, 2H), 7.49 (s, 1H), 7.33 (dd, J = 9.2, 2.4 Hz, 1H), 7.19 (d, J = 2.4 Hz, 1H), 7.02 (d, J = 8.8 Hz, 2H), 6.70 (dd, J = 7.2, 1.6 Hz, 1H), 2.99–2.85 (m, 5H), 2.79 (s, 2H), 1.80 (m, 3H), 1.64 (m, 4H), 1.30 (m, 4H), 1.18 (m, 9H), 1.03–0.97 (m, 2H), 0.85 (m, 4H) ppm; ^{13}C NMR (101 MHz, DMSO-d_6) δ: 167.73, 164.09, 158.68, 155.65, 151.84, 138.94, 134.09, 132.07, 130.42, 128.61, 126.33, 125.51, 124.32, 123.74, 123.48, 122.83, 118.70, 118.15, 116.07, 114.57, 114.02, 112.81, 112.41, 45.83, 29.49, 29.12, 27.35, 25.65, 22.56, 22.20, 21.47, 14.42, 14.16, 13.02 ppm; HRMS: ([M]$^+$) Calcd for $C_{40}H_{45}ClN_5O_2$: 622.3256; found: 622.3266.

4. Conclusions

In summary, a NIR ratiometric fluorescent probe **IPB-RL-1** with an ultra-large Stokes shift (460 nm) that is superior to most reported probes has been developed. **IPB-RL-1** shows high sensitivity and selectivity. Detection of SO_2 in mitochondria in living SKOV-3 cells was also realized. Moreover, the probe was successfully used to detect SO_2 in zebrafish which may be useful for the understanding of biological roles of SO_2 in mitochondria and in vivo. However, due to the small overlap between donor emission and acceptor absorption of the probe **IPB-RL-1**, the fluorescence transfer efficiency is only 51%, which implies that in order to obtain a high fluorescence transfer efficiency, the overlap effect between donor emission and acceptor absorption, in addition to the distance between donor and acceptor, should be carefully considered for the FRET-based probe design in the future.

Supplementary Materials: Supplementary data associated with this article can be found in the online version. The following supporting information can be downloaded at: https://www.mdpi.com/article/10.3390/molecules28020515/s1, Figure S1: Ratiometric fluorescence responses F_{475}/F_{760} of **IPB-RL-1** upon the addition of 10 equiv. SO_3^{2-} in the presence of 100 eq. background ions (1, probe; 2, SO_4^{2-}; 3, Br^-; 4, ACO^-; 5, Cl^-; 6, ClO^-; 7, Cys; 8, ClO_4^-; 9, GSH; 10, F^-; 11, $H_2PO_4^-$; 12, HCO_3^-; 13, HPO_4^{2-}; 14, HS^-; 15, I^-; 16, NO_2^-; 17, NO_3^-; 18, $S_2O_8^{2-}$; 19, SO_3^{2-}); Figure S2: Relationship between fluorescence intensity ratio (F_{475}/F_{760}) and SO_3^{2-} concentration; Figure S3: Time dependent increase of **IPB-RL-1** fluorescence intensities after addition of SO_3^{2-}; Figure S4: Cytotoxicity of **IPB-RL-1**; Figure S5: Normalized emission spectra of donor (compound **3**) and normalized absorption spectra of **IPB-RL-1**; Figure S6: The emission spectrum of probe **IPB-RL-1** and donor; Figures S7–S13: ^{1}H NMR, ^{13}C NMR, HRMS of related compounds; Table S1: Comparison with other probes [31–57].

Author Contributions: Conceptualization, R.C. and C.L.; methodology, C.L.; software, P.Z.; validation, R.C., C.L. and P.Z.; formal analysis, Y.G.; investigation, Y.G.; resources, Y.G.; data curation, K.Q.; writing—original draft preparation, K.Q.; writing—review and editing, Y.G.; visualization, Y.G.; supervision, Y.G. All authors have read and agreed to the published version of the manuscript.

Funding: This research was supported by the Natural Science Foundation of Shandong Province (ZR2021MB033), the Incubation Program of Youth Innovation of Shandong Province, and the Innovative Research Programs of Higher Education of Shandong Province (2019KJC009).

Institutional Review Board Statement: Not applicable.

Informed Consent Statement: Not applicable.

Data Availability Statement: The data that support the findings of this study are available from the corresponding author upon reasonable request.

Conflicts of Interest: The authors declare no conflict of interest.

References

1. Lin, V.S.; Chen, W.; Xian, M.; Chang, C.J. Chemical probes for molecular imaging and detection of hydrogen sulfide and reactive sulfur species in biological systems. *Chem. Soc. Rev.* **2015**, *44*, 4596–4618. [CrossRef] [PubMed]
2. Jiao, X.; Li, Y.; Niu, J.; Xie, X.; Wang, X.; Tang, B. Small-Molecule Fluorescent Probes for Imaging and Detection of Reactive Oxygen, Nitrogen, and Sulfur Species in Biological Systems. *Anal. Chem.* **2018**, *90*, 533–555. [CrossRef] [PubMed]
3. Wu, L.; Sedgwick, A.C.; Sun, X.; Bull, S.D.; He, X.-P.; James, T.D. Reaction-Based Fluorescent Probes for the Detection and Imaging of Reactive Oxygen, Nitrogen, and Sulfur Species. *Acc. Chem. Res.* **2019**, *52*, 2582–2597. [CrossRef] [PubMed]
4. Li, K.; Li, L.-L.; Zhou, Q.; Yu, K.-K.; Kim, J.S.; Yu, X.-Q. Reaction-based fluorescent probes for SO_2 derivatives and their biological applications. *Co-ord. Chem. Rev.* **2019**, *388*, 310–333. [CrossRef]
5. Liu, A.; Ji, R.; Shen, S.; Cao, X.; Ge, Y. A ratiometric fluorescent probe for sensing sulfite based on a pyrido[1,2-a]benzimidazole fluorophore. *New J. Chem.* **2017**, *41*, 10096–10100. [CrossRef]
6. Ma, C.; Zhang, L.; Hou, L.; Chen, F.; Liu, A.; Ji, R.; Wang, Q.; Yuan, C.; Ge, Y. A fluorescent probe with a large Stokes shift for sensing sulfite in dry white wine based on pyrazolo[1,5-a]pyridine fluorophore. *Tetrahedron Lett.* **2021**, *76*, 153210. [CrossRef]
7. Duan, G.Y.; Wang, H.; Sun, H.; Yuan, C.; Xu, Z.; Ge, Y.Q. Near-infrared TBET cassette with ultra large stokes shift and its application for SO_2 imaging in cells. *Chem. Eng. J. Adv.* **2021**, *8*, 100141. [CrossRef]
8. Cui, R.; Gao, Y.; Ge, H.; Shi, G.; Li, Y.; Liu, H.; Ma, C.; Ge, Y.; Liu, C. A turn-on fluorescent probe based on indolizine for the detection of sulfite. *New J. Chem.* **2022**, *46*, 8088–8093. [CrossRef]
9. Zhang, W.; Huo, F.; Zhang, Y.; Chao, J.; Yin, C. Mitochondria-targeted NIR fluorescent probe for reversible imaging H2O2/SO_2 redox dynamics in vivo. *Sens. Actuators B* **2019**, *297*, 126747. [CrossRef]
10. Ren, H.; Huo, F.; Wu, X.; Liu, X.; Yin, C. An ESIPT-induced NIR fluorescent probe to visualize mitochondrial sulfur dioxide during oxidative stress *in vivo*. *Chem. Commun.* **2021**, *57*, 655–658. [CrossRef]
11. He, L.; Yang, Y.; Lin, W. Rational Design of a Rigid Fluorophore–Molecular Rotor-Based Probe for High Signal-to-Background Ratio Detection of Sulfur Dioxide in Viscous System. *Anal. Chem.* **2019**, *91*, 15220–15228. [CrossRef] [PubMed]
12. Gao, W.; Ma, Y.; Lin, W. Design of a FRET-based fluorescent probe for the reversible detection of $SO_2$and formaldehyde in living cells and mice. *New J. Chem.* **2020**, *44*, 13654–13658. [CrossRef]
13. Wu, L.; Huang, C.; Emery, B.P.; Sedgwick, A.C.; Bull, S.D.; He, X.-P.; Tian, H.; Yoon, J.; Sessler, J.L.; James, T.D. Förster resonance energy transfer (FRET)-based small-molecule sensors and imaging agents. *Chem. Soc. Rev.* **2020**, *49*, 5110–5139. [CrossRef] [PubMed]
14. Yuan, L.; Lin, W.; Zheng, K.; Zhu, S. FRET-Based Small-Molecule Fluorescent Probes: Rational Design and Bioimaging Applications. *Acc. Chem. Res.* **2013**, *46*, 1462–1473. [CrossRef] [PubMed]
15. Lee, M.H.; Kim, J.S.; Sessler, J.L. Small molecule-based ratiometric fluorescence probes for cations, anions, and biomolecules. *Chem. Soc. Rev.* **2015**, *44*, 4185–4191. [CrossRef]
16. Tan, L.; Ding, H.; Chanmungkalakul, S.; Peng, L.; Yuan, G.; Yang, Q.; Liu, X.; Zhou, L. A smart TP-FRET-based ratiometric fluorescent sensor for bisulfite/formaldehyde detection and its imaging application. *Sens. Actuators B* **2021**, *345*, 130331. [CrossRef]
17. Zhu, X.; Zhu, L.; Liu, H.-W.; Hu, X.; Peng, R.-Z.; Zhang, J.; Zhang, X.-B.; Tan, W. A two-photon fluorescent turn-on probe for imaging of SO_2 derivatives in living cells and tissues. *Anal. Chim. Acta* **2016**, *937*, 136–142. [CrossRef]
18. Shen, W.; Xu, H.; Feng, J.; Sun, W.; Hu, G.; Hu, Y.; Yang, W. A ratiometric and colorimetric fluorescent probe designed based on FRET for detecting SO32−/HSO3− in living cells and mice. *Spectrochim. Acta Part A* **2021**, *263*, 120183. [CrossRef]
19. Liu, W.; Zhang, D.; Ni, B.; Li, J.; Weng, H.; Ye, Y. Mitochondria-targeted and FRET based ratiometric fluorescent probe for SO_2 and its cell imaging. *Sens. Actuators B* **2019**, *284*, 330–336. [CrossRef]
20. Zhang, W.; Huo, F.; Cheng, F.; Yin, C. Employing an ICT-FRET Integration Platform for the Real-Time Tracking of SO_2 Metabolism in Cancer Cells and Tumor Models. *J. Am. Chem. Soc.* **2020**, *142*, 6324–6331. [CrossRef]

21. Huang, Y.; Zhang, Y.; Huo, F.; Chao, J.; Yin, C. A dual-targeted organelles SO_2 specific probe for bioimaging in related diseases and food analysis. *Chem. Eng. J.* **2022**, *433*, 133750. [CrossRef]
22. Huang, M.-F.; Chen, L.-N.; Ning, J.-Y.; Wu, W.-L.; He, X.-D.; Miao, J.-Y.; Zhao, B.-X. A new lipid droplets-targeted fluorescence probe for specific detection of SO_2 derivatives in living cells. *Sens. Actuators B* **2018**, *261*, 196–202. [CrossRef]
23. Yan, Y.-H.; Cui, X.-L.; Li, Z.-Y.; Ding, M.-M.; Che, Q.-L.; Miao, J.-Y.; Zhao, B.-X.; Lin, Z.-M. A synergetic FRET/ICT platform-based fluorescence probe for ratiometric imaging of bisulfite in lipid droplets. *Anal. Chim. Acta* **2020**, *1137*, 47–55. [CrossRef]
24. Sun, W.-X.; Li, N.; Li, Z.-Y.; Yuan, Y.-C.; Miao, J.-Y.; Zhao, B.-X.; Lin, Z.-M. A mitochondria-targeted ratiometric fluorescence probe for detection of SO_2 derivatives in living cells. *Dye. Pigment.* **2020**, *182*, 108658. [CrossRef]
25. Liu, F.-T.; Li, N.; Chen, Y.-S.; Yu, H.-Y.; Miao, J.-Y.; Zhao, B.-X. A quinoline-coumarin near-infrared ratiometric fluorescent probe for detection of sulfur dioxide derivatives. *Anal. Chim. Acta* **2022**, *1211*, 339908. [CrossRef]
26. Sun, W.; Guo, S.; Hu, C.; Fan, J.; Peng, X. Recent Development of Chemosensors Based on Cyanine Platforms. *Chem. Rev.* **2016**, *116*, 7768–7817. [CrossRef]
27. Zhang, D.; Liu, A.; Ji, R.; Dong, J.; Ge, Y. A mitochondria-targeted and FRET-based ratiometric fluorescent probe for detection of SO_2 derivatives in water. *Anal. Chim. Acta* **2018**, *1055*, 133–139. [CrossRef]
28. Song, G.; Liu, A.; Jiang, H.; Ji, R.; Dong, J.; Ge, Y. A FRET-based ratiometric fluorescent probe for detection of intrinsically generated SO_2 derivatives in mitochondria. *Anal. Chim. Acta* **2018**, *1053*, 148–154. [CrossRef]
29. Chen, F.; Liu, A.; Ji, R.; Xu, Z.; Dong, J.; Ge, Y. A FRET-based probe for detection of the endogenous SO_2 in cells. *Dye. Pigment.* **2019**, *165*, 212–216. [CrossRef]
30. Ge, Y.; Ji, R.; Shen, S.; Cao, X.; Li, F. A ratiometric fluorescent probe for sensing Cu2+ based on new imidazo[1,5-a]pyridine fluorescent dye. *Sens. Actuators B* **2017**, *245*, 875–881. [CrossRef]
31. Yan, Y.; He, X.; Miao, J.; Zhao, B. A near-infrared and mitochondria-targeted fluorescence probe for ratiometric monitoring of sulfur dioxide derivatives in living cells. *J. Mater. Chem. B.* **2019**, *7*, 6585–6591. [CrossRef]
32. Shen, R.; Qian, Y. A novel ratiometric fluorescent probe for specific detection of HSO_3^- at nanomolar level through 1,4-Michael addition. *J. Photochem. Photobiol. A.* **2020**, *387*, 112110. [CrossRef]
33. Wu, W.; Ma, H.; Huang, M.; Miao, J.; Zhao, B. Mitochondria-targeted ratiometric fluorescent probe based on FRET for bisulfite. *Sens. Actuators, B.* **2017**, *241*, 239–244. [CrossRef]
34. Yang, D.; Ning, J.; Wu, X.; Yao, W.; Shi, H.; Miao, J.; Zhao, B.; Lin, Z. Ratiometric fluorescence sensing of endogenous sulfur dioxide derivatives: Bio-imaging application in lipid droplets. *Dyes Pigm.* **2021**, *192*, 109457. [CrossRef]
35. Li, D.; Wang, Z.; Cui, J.; Wang, X.; Miao, J.; Zhao, B. A new fluorescent probe for colorimetric and ratiometric detection of sulfur dioxide derivatives in liver cancer cells. *Sci. Rep.* **2017**, *7*, 45294. [CrossRef]
36. Zhao, J.; Huang, L.; Yan, M.; Qu, Y.; Feng, H.; Sun, Y. A lysosome specific ratiometric fluorescent probe for detection of bisulfite ion based on hybrid coumarin-benzimidazolium compounds. *Phosphorus. Sulfur.* **2021**, *196*, 321–327. [CrossRef]
37. Shen, R.; Qian, Y. A mitochondria-oriented fluorescent probe for ultrafast and ratiometric detection of HSO_3^- based on naphthalimide–hemicyanine. *New J. Chem.* **2019**, *43*, 7606–7612. [CrossRef]
38. Wang, Y.; Meng, Q.; Zhang, R.; Jia, H.; Wang, C.; Zhang, Z. A mitochondria-targeted ratiometric probe for the fluorescent and colorimetric detection of SO_2 derivatives in live cells. *J. Lumin.* **2017**, *192*, 297–302. [CrossRef]
39. Liu, K.; Chen, Y.; Sun, H.; Wang, S.; Kong, F. Construction of a novel near-infrared fluorescent probe with multiple fluorescence emission and its application for SO_2 derivative detection in cells and living zebrafish. *J. Mater. Chem. B.* **2018**, *6*, 7060–7065. [CrossRef]
40. Yang, D.; He, X.; Wu, X.; Shi, H.; Miao, J.; Zhao, B.; Lin, Z. A novel mitochondria-targeted ratiometric fluorescent probe for endogenous sulfur dioxide derivatives as a cancer-detecting tool. *J. Mater. Chem. B.* **2020**, *8*, 5722–5728. [CrossRef]
41. Yin, G.; Gan, Y.; Yu, T.; Niu, T.; Yin, P.; Chen, H.; Zhang, Y.; Li, H.; Yao, S. A dual-emission and mitochondria-targeted fluorescent probe for rapid detection of SO_2 derivatives and its imaging in living cells. *Talanta.* **2019**, *191*, 428–434. [CrossRef]
42. Huang, Y.; Zhang, Y.; Huo, F.; Yin, C. FRET-dependent single/two-channel switch endowing a dual detection for sulfite and its organelle targeting applications. *Dyes Pigm.* **2021**, *184*, 108869. [CrossRef]
43. Wang, M.; Liu, Q.; Sun, X.; Zheng, S.; Ma, Y.; Wang, Y.; Yan, M.; Lu, Z.; Fan, C.; Lin, W. Ratiometric and reversible detection of endogenous SO_2 and HCHO in living cells and mice by a near-infrared and dual-emission fluorescent probe. *Sensors Actuators B Chem.* **2021**, *335*, 129649. [CrossRef]
44. Zhang, L.; Wang, Z.; Liu, J.; Miao, J.; Zhao, B. A rational design of ratiomet-ric fluorescent probes based on new ICT/FRET platform and imaging of endogenous sulfite in living cells. *Sens. Actuators, B.* **2017**, *253*, 19–26. [CrossRef]
45. Song, G.; Luo, J.; Xing, X.; Ma, H.; Yang, D.; Cao, X.; Ge, Y.; Zhao, B. A ratiometric fluorescence probe for rapid detection of mitochondrial SO_2 derivatives. *New J. Chem.* **2018**, *42*, 3063–3068. [CrossRef]
46. Li, D.; Han, X.; Yan, Z.; Cui, Y.; Miao, J.; Zhao, B. A far-red ratiometric fluorescent probe for SO_2 derivatives based on the ESIPT enhanced FRET platform with improved performance. *Dyes Pigm.* **2018**, *151*, 95–101. [CrossRef]
47. Yan, Y.; Wu, Q.; Che, Q.; Ding, M.; Xu, M.; Miao, J.; Zhao, B.; Lin, Z. A mitochondria-targeted fluorescent probe for the detection of endogenous SO_2 derivatives in living cells. *Analyst.* **2020**, *145*, 2937–2944. [CrossRef]
48. Li, D.; Wang, Z.; Su, H.; Miao, J.; Zhao, B. Fluorescence detection of endogenous bisulfite in liver cancer cells using an effective ESIPT enhanced FRET platform. *Chem. Commun.* **2017**, *53*, 577–580. [CrossRef]

49. Lu, Y.; Dong, B.; Song, W.; Sun, Y.; Mehmood, A.; Lin, W. A mitochondria-targeting ratiometric fluorescent probe for the detection of sulfur dioxide in living cells. *New J. Chem.* **2020**, *44*, 11988–11992. [CrossRef]
50. Li, Z.; Cui, X.; Yan, Y.; Che, Q.; Miao, J.; Zhao, B.; Lin, Z. A novel endoplasmic reticulum-targeted ratiometric fluorescent probe based on FRET for the detection of SO_2 derivatives. *Dyes Pigm.* **2021**, *188*, 109180. [CrossRef]
51. Li, D.; Wang, Z.; Cao, X.; Cui, J.; Wang, X.; Cui, H.; Miao, J.; Zhao, B. A mitochondria-targeted fluorescent probe for ratiometric detection of endogenous sulfur dioxide derivatives in cancer cells. *Chem. Commun.* **2016**, *52*, 2760–2763. [CrossRef]
52. Zhang, G.; Ji, R.; Kong, X.; Ning, F.; Liu, A.; Cui, J.; Ge, Y. A FRET based ratiometric fluorescent probe for detection of sulfite in food. *RSC Adv.* **2019**, *9*, 1147–1150. [CrossRef]
53. Yang, Y.; He, L.; Xu, K.; Lin, W. Development of a mitochondria-targeted fluorescent probe for the ratiometric visualization of sulfur dioxide in living cells and zebrafish. *Anal. Methods.* **2019**, *11*, 3931–3935. [CrossRef]
54. Shen, W.; Xu, H.; Feng, J.; Sun, W.; Hu, G.; Yang, W. A ratiometric and colorimetric fluorescent probe designed based on FRET for detecting ${SO_3}^{2-}/HSO_3^-$ in living cells and mice. *Spectrochim. Acta, Part A.* **2021**, *263*, 120183. [CrossRef]
55. Yang, X.; Zhou, X.; Zhang, S.; Yang, Y.; Chen, J.; Guo, X.; Li, Z.; Yang, R.; Zhou, Y. A TP-FRET-based two-photon fluorescent probe for ratiometric visualization of endogenous sulfur dioxide derivatives in mitochondria of living cells and tissues. *Chem. Commun.* **2016**, *52*, 10289–10292. [CrossRef]
56. Li, T.; Huo, F.; Chao, J.; Yin, C. Independent bi-reversible reactions and regulable FRET efficiency achieving real-time visualization of Cys metabolizing into SO_2. *Chem. Commun.* **2020**, *56*, 11453–11456. [CrossRef]
57. Chen, X.; Chen, Q.; He, D.; Yang, S.; Yang, Y.; Qian, J.; Long, L.; Wang, K. Mitochondria targeted and immobilized ratiometric NIR fluorescent probe for investigating SO_2 phytotoxicity in plant mitochondria. *Sens. Actuators, B.* **2022**, *370*, 132433. [CrossRef]